

---

## Sub-axial deformation in oceanic lower crust: Insights from seismic reflection profiles in the Enderby Basin and comparison with the Oman ophiolite

Sauter Daniel <sup>1,\*</sup>, Werner Philippe <sup>1</sup>, Ceuleneer Georges <sup>2</sup>, Manatschal Gianreto <sup>1</sup>, Rospabe Mathieu <sup>3</sup>, Tugend Julie <sup>4</sup>, Gillard Morgane <sup>4</sup>, Autin Julia <sup>1</sup>, Ulrich Marc <sup>1</sup>

<sup>1</sup> Univ Strasbourg, Inst Phys Globe Strasbourg IPGS, UMR7516 CNRS, 1 Rue Blessig, F-67084 Strasbourg, France.

<sup>2</sup> Univ Toulouse, Observ Midi Pyrenees, CNRS, Geosci Environm Toulouse GET,IRD, 14 Ave E Belin, F-31400 Toulouse, France.

<sup>3</sup> Japan Agcy Marine Earth Sci & Technol JAMSTEC, Res Inst Marine Geodynam IMG, 2-15 Natsushima, Yokosuka, Kanagawa 2370061, Japan.

<sup>4</sup> Sorbonne Univ, Inst Sci Terre Paris IStEP, CNRS, UMR 7193, 4 Pl Jussieu, F-75005 Paris, France.

\* Corresponding author : Daniel Sauter, email address : [daniel.sauter@unistra.fr](mailto:daniel.sauter@unistra.fr)

---

### Abstract :

We analyzed high-quality seismic reflection profiles across the ocean-continent transition in the Enderby Basin between the Kerguelen Plateau and the Antarctic margin. There, we observe numerous high-amplitude dipping reflections in the lower oceanic crust which was accreted at a magmatic spreading center as testified by the almost uniform 6.4-7 km thick crust and its unfaulted, flat top basement. The deep reflections are rooting onto the Moho and are dipping both ridgeward and continentward. They occur in dense networks in mature oceanic crust as well as close to the continentward termination of oceanic crust and in the ocean-continent transition zone. The comparison with field observations in the Oman ophiolite suggests that these lower crustal dipping reflectors could correspond to syn-magmatic faults. In Oman, very high temperature (up to syn-magmatic), high temperature (sub-solidus plastic deformation) and low temperature (brittle) deformation coexist along the same fault over distances of a few hundred meters at Moho level. This very high temperature gradient may be explained by the sudden and intense interaction between crystallizing magmas and hydrothermal fluids induced by the episodic nucleation of faults in a context of continuous magmatic spreading. The igneous layering becomes extremely irregular compared to its monotonous sub-horizontal orientation away from the faults which, together with enhanced hydrothermal alteration restricted to the fault zones, might change the physical properties (velocity, density) and increase the reflectivity of syn-magmatic faults. We further speculate that these processes could explain the brightness of the lower crustal dipping reflectors observed in our seismic reflection data. Both the seismic reflection profiles of the Enderby Basin and the Oman ophiolite show evidence for syn-accretion tectonism at depth together with the systematic rotation of originally horizontal lava flows or originally vertical dikes, pre-dating cessation of magmatic activity. This indicates ubiquitous deformation processes within the axial zone of magmatic spreading centers.

---

## Highlights

► High amplitude dipping reflections are observed in the lower [oceanic crust](#) in the Enderby Basin. ►  
The comparison with the Oman [ophiolite](#) suggests that they correspond to syn-magmatic faults. ►  
Deformation processes are ubiquitous within the axial zone of magmatic spreading centers.

**Keywords** : lower oceanic crust, oceanic accretionary processes, dipping reflectors, ocean-continent transition, Enderby Basin, Oman ophiolite



## 51 **1. Introduction**

52 Most of the oceanic crust created over the last 200 million years formed at  
53 intermediate- to fast-spreading mid-ocean ridges (50-200 km/Ma full rate) (Karson,  
54 2002). Despite the widespread occurrence of such magmatic crust, direct  
55 observations of its lower part made essentially of gabbroic cumulates are particularly  
56 scarce. There are only two locations (Hess Deep and Pito Deep in the Pacific Ocean)  
57 where *in situ* fast-spread plutonic crust is exposed in response to ridge propagation.  
58 Rocks from such deep horizons have been collected by submersible, remotely  
59 operated underwater vehicle and drilling, the section recovered by drilling being  
60 typically several tens of meter in length only (e.g. Brown et al., 2019; Gillis et al.,  
61 2014). No *in situ* observations within the lowermost oceanic crust accreted at fast-  
62 spreading ridges have been made elsewhere, apart from some sites in large offset  
63 transform faults, where crustal structures might not be representative of standard  
64 accretion processes (cf. Constantin et al., 1996).

65 Therefore, our knowledge of the deep crustal magmatic system along fast-spreading  
66 mid-oceanic ridges is mostly derived from seismic studies of the East Pacific Rise  
67 (EPR) and ancient analogues (e.g. ophiolites) although the tectonic setting of their  
68 genesis is still debated (MacLeod et al., 2013). Seismic reflection data have shown  
69 that there is a near static region of high melt proportions, the axial magma lens  
70 (AML), 1-3 km wide and a few hundred meters high, at a depth of 1-2 km beneath the

71 ridge axis, for much of its length (e.g. Detrick et al., 1987). Beneath the AML,  
72 tomographic studies have indicated that there is a low velocity zone a few kilometers  
73 wide (e.g. Toomey et al., 1990), which is inferred to consist of a crystal mush, i.e.  
74 incompletely crystallized cumulates (Sinton and Dietrick, 1992). More recent seismic  
75 reflection studies have shown a series of melt lenses in the lower crust below the  
76 AML both on and off-axis (e.g. Marjanovic et al., 2014). In addition, melt in the lower  
77 crust and/or the crust-mantle transition zone was also inferred by seafloor  
78 compliance studies (Crawford and Webb, 2002). Thus, there is an increasing set of  
79 arguments for a multi-level complex of melt lenses beneath the ridge axis (Marjanovic  
80 et al., 2014).

81 However, how these melt lenses contribute to the formation of both the upper and  
82 lower crust and what accretion processes are operating in the lower crust remain  
83 unclear. Two end-member models for crustal accretion have emerged from  
84 geophysical observations at fast-spreading ridges and more largely from field  
85 evidence in the Oman and other ophiolites (Kelemen et al., 1997; Marjanovic et al.,  
86 2014; Nicolas and Boudier, 2015). In the 'gabbro glacier' model, most crystal growth  
87 occurs within the AML, which subsides by ductile flow to form the entire gabbro  
88 section (e.g. Quick and Delinger, 1993). The 'sheeted sill' model, where gabbro  
89 formation occurs *in situ* in small magma bodies throughout the lower oceanic crust,  
90 better fits with the occurrence and structure of the interlayered mafic and ultramafic  
91 cumulates in ophiolites (Kelemen et al., 1997). In the Oman ophiolite, recent studies  
92 of the crust-mantle transition zone have shown that faults, enabling water introduction  
93 at depth, may be a more common feature than previously expected in the formation  
94 of the lowermost oceanic crust in a context of high melt supply (Abily et al., 2011;  
95 Rospabé et al., 2019). Such faults have not been documented yet in seismic

96 reflection profiles at fast-spreading ridges. However, lower crustal dipping reflectors  
97 have been observed on ridge flanks within both slow- and fast-spreading crust (see  
98 Bécél et al. (2015) for a review) while they are not imaged along the ridge axis itself.  
99 Such lower crustal dipping reflections within fast-spread crust have been interpreted  
100 as arising from shear zones that form near the spreading center in the region with  
101 interstitial melt, and result from shear at the base of the crust (Bécél et al., 2015). It  
102 has been further suggested that such differential motion at the base of the crust  
103 could result from plate reorganizations (Bécél et al., 2015).

104 While lower crustal events dipping toward the paleo-ridge axis have been  
105 predominantly described until now (Bécél et al., 2015; Ding et al., 2018; Reston et al.,  
106 1999), here we identify numerous both ridgeward and continentward dipping high-  
107 amplitude reflectors in the lower oceanic crust of the Enderby Basin, between the  
108 Kerguelen Plateau and the Antarctic margin. Thanks to high-quality seismic reflection  
109 profiles, we are able to document the occurrence of such dipping reflections in two  
110 different but juxtaposed domains: typical oceanic crust and the ocean-continent  
111 transition. We relate these lower crustal dipping reflectors to syn-magmatic faulting  
112 described recently in the Oman ophiolite (Abily et al., 2011; Rospabé et al., 2019).  
113 These observations give some clues for the sub-axial tectono-magmatic processes  
114 that may occur within the oceanic crust.

## 115 **2. Geological background**

### 116 **2.1. The Enderby Basin**

117 Here, we focus on the oceanic domain and the ocean-continent transition within the  
118 central part of the Enderby Basin. It is bounded by the Enderby Land to the  
119 southwest, by the Elan Bank to the north and the southern Kerguelen Plateau to the

120 northeast, by the Princess Elizabeth Trough to the east and by the Antarctic margin  
121 and the Mac Robertson Land to the south (Fig. 1). The Enderby Basin is thought to  
122 be formed during the Early Cretaceous as East Antarctica and India rifted apart  
123 (McElhinny, 1970). An intermediate spreading rate of ~60 km/Ma has been inferred  
124 from east-west trending magnetic anomalies M4 (126.7 Ma), M2 (124.1 Ma), and M0  
125 (120.4 Ma) (Gibbons et al., 2013). These anomalies have been identified north and  
126 south of an extinct ridge running parallel to the Elan Bank (Gaina et al., 2007)  
127 (Fig. 1). However, this extinct ridge is poorly constrained and, contrasting with many  
128 other extinct ridges, it is not linked to a gravity low (MacLeod et al., 2017). Moreover,  
129 magnetic anomaly profiles in the Enderby Basin are scarce and, due to the absence  
130 of clear and continuous magnetic anomalies, their identification is debated (e.g.  
131 Golynsky et al., 2013). It has been suggested that the lack of clear magnetic  
132 anomalies may result from seafloor spreading during the Cretaceous Normal  
133 Superchron (Jokat et al., 2010). Therefore, no consensus about the spreading history  
134 of the Enderby Basin has been reached yet (e.g. Davis et al., 2018).

135 By contrast, there is a consensus about the location of the inboard edge of  
136 unequivocal oceanic crust (LOC) (Fig. 1). It typically coincides with: (1) a prominent  
137 oceanward step-up in the basement level of 500-1000 m, (2) the continentward  
138 abrupt termination of a well-marked oceanic Moho in the seismic reflection profiles  
139 (Stagg et al., 2005), and (3) the Enderby Basin Anomaly (EBA; (Golynsky et al.,  
140 2013), a high-amplitude (350–500 nT) magnetic anomaly which is interpreted to mark  
141 the contact between strongly magnetized oceanic crust and less magnetized  
142 continental rocks (Golynsky et al., 2013). The domain to the north of the LOC is  
143 described as unambiguous oceanic crust (Stagg et al., 2005). The domain  
144 immediately to the south, within the ocean-continent transition, is referred to as

145 transitional crust on the basis of seismic reflection profiles and limited refraction data  
146 (sonobuoys) (Stagg et al., 2005). It is thought to be made of stretched continental  
147 crust or exhumed mantle that was subsequently modified by magmatic intrusions  
148 during the formation of the initial- or proto-oceanic crust (Gaina et al., 2007; Gillard et  
149 al., 2019).

150 We use 10 high-resolution and deep-penetrating seismic reflection profiles from the  
151 GA-228 and GA-229 surveys collected by Geoscience Australia in 2000 and 2001,  
152 respectively (Stagg et al., 2005). During these surveys, 36-fold stacked and migrated  
153 deep seismic data (60 l airgun array source; 3600 m streamer; 288 channels; 16 s  
154 record length) were recorded between offshore western Enderby Land and the  
155 southern Kerguelen Plateau (Fig. 1) (Stagg et al., 2005). The seismic profiles are  
156 trending North-South, perpendicular to the LOC and the magnetic lineations of the  
157 Enderby Basin. They are thus thought to be collected along a flow line of the Enderby  
158 Basin spreading center, although the geometry and segmentation of this ridge is  
159 poorly known. This data set was used by Stagg et al. (2005) to map and describe  
160 distinct sectors along the Antarctic margin and the adjacent oceanic crust.

## 161 **2.2. The Oman ophiolite**

162 The Oman ophiolite is the largest coherent remaining fragment of the Tethyan  
163 oceanic lithosphere. It is interpreted as formed along a highly productive (Ceuleneer  
164 et al., 1996; Pallister and Hopson, 1981) and possibly fast-spreading center ~95-97  
165 million years ago (Boudier et al., 1985; Rioux et al., 2012). Major ductile shear zones  
166 were recognized as common features in the mantle and crustal sections of the Oman  
167 ophiolite since pioneer structural studies (Amri et al., 1996; Boudier et al., 1985;  
168 Boudier et al., 1988; Joussetin and Nicolas, 2000; Joussetin et al., 1998). They are

169 characterized by intense deformation with the development of peridotite mylonites  
170 and flaser gabbros on thicknesses ranging from a few meters to several hundred  
171 meters. The main ones can be followed along strike over distances of several tens of  
172 kilometres. Shearing initiated at very high temperature, close or above the solidus of  
173 peridotites and gabbros, frequently in the presence of melt, and usually stopped  
174 before the rock cooled down significantly, although most of these shear zones were  
175 still active at greenschist facies metamorphic conditions.

176 The shear zones revealed by the early structural mapping of the Oman ophiolite  
177 show a clear continuity with the metamorphic sole and, hence, have been attributed  
178 to emplacement tectonics (intra-oceanic thrusting close to the ridge axis) (Boudier et  
179 al., 1985; Boudier et al., 1988). Until recently, this interpretation was extended by  
180 most geologists to all kinds of ductile and brittle fault zones affecting the mantle and  
181 the deep crustal section of the Oman ophiolite, apart from minor ones interpreted in  
182 terms of oceanic spreading (e.g. Dijkstra et al., 2002). Circularity in the way of  
183 reasoning maintained the confusion: Oman ophiolite being supposed to derive from a  
184 fast-spreading centre where faulting (at least down to deep levels of the crust) was  
185 supposed to play an anecdotic role relative to igneous accretion, faults observed in  
186 Oman were *a priori* attributed to later events, among other the intra-oceanic thrusting.  
187 However, more detailed studies have revealed the existence of high temperature  
188 shear zones, which did not record strike slip or inverse kinematics calling for  
189 convergent tectonics. A normal shear sense is actually recorded by many faults  
190 among those which have an azimuth subparallel to the one of paleo-ridge axis,  
191 including high temperature ductile faults (Abily et al., 2011; Rospabé et al., 2019).

192 Moreover, our structural observations and petrological data from the Maqsad area  
193 highlight that faults were active early at Moho level, since the magmatic stage, and

194 that they contributed to the petrological and geochemical organization of the lower  
195 crust. Due to the deep introduction of water they triggered, these faults exerted a  
196 strong control on the reaction leading to the transformation of mantle harzburgite into  
197 dunite at the Moho and on melts migration and crystallization paths, and continued to  
198 serve as major avenues for hydrothermal fluids down to lower temperatures (Abily et  
199 al., 2011; Rospabé et al., 2017). These faults are either parallel to the strike of the  
200 sheeted dike complex (*i.e.* parallel to the regional orientation of the inferred paleo-  
201 ridge axis) or slightly oblique to it (Rospabé et al., 2019). They mostly have a  
202 ridgeward dip ranging from 65° to 10° and some are clearly listric, with dips  
203 progressively shallowing as the crust-mantle boundary is approached, inducing early  
204 tilting of blocks of hardly consolidated layered cumulates (Fig. 2). Normal syn-  
205 accretion faults highly altered in a wide temperature range have been identified in  
206 other massifs of the Oman ophiolite (e.g. Zihlmann et al., 2018) and seem to be the  
207 rule rather than the exception. In the case of the fault studied in detail by Abily et al.  
208 (2011), the rotation of these blocks of layered cumulates, at high angles relative to  
209 the Moho, was accommodated by an anastomosing fault network connected to the  
210 main fault plane. It is locally underlined by thin screens of gabbroic micropegmatites,  
211 which represent former hydrated evolved melts crystallizing as amphibole-bearing  
212 gabbros and by ptigmatic folds, pointing to viscous deformation of a sheared and  
213 compacting crystal mush (Abily et al., 2011) (Fig. 2). Flat-lying undeformed cumulate  
214 layers, in the same differentiation stage as the deformed ones, settled directly over  
215 the tilted blocks, which is the main evidence for syn-magmatic block rotation (Fig. 2).  
216 In this example, outcrops witnessing syn-magmatic deformation exceptionally  
217 escaped lower temperature deformation and alteration. This evidences a remarkable  
218 lateral evolution in the deformation style on a distance of a few hundred meters.

219 Moving away from the zone where syn-magmatic structures are preserved, i.e.  
220 moving toward the main fault that was active down to greenschist facies conditions,  
221 shearing continued at sub-solidus temperatures along some fault planes, and brittle  
222 deformation structures become more and more prevalent (Abily et al., 2011).

223 Lower crustal gabbros from Oman generally present a quite regular igneous (modal)  
224 layering sub-parallel to the crust-mantle boundary (“paleo-Moho”). This monotonous  
225 orientation is totally disturbed within several hundred meters from these syn-  
226 magmatic normal faults. Minor faults are spaced by a characteristic distance of  
227 ~250 m on average, but the major ones may be several kilometers apart. Moving  
228 from the top to the base of the crust-mantle transition zone, the deformation  
229 conditions evolved from brittle to ductile. Most of these faults were active in a broad  
230 temperature interval, with the development of serpentine and carbonate breccias that  
231 can be intruded by gabbroic dikes altered in greenschist facies conditions. These  
232 brecciated zones reach up to 10 m in thickness in the few major faults and have been  
233 zones of intense fluid circulation (Rospabé et al., 2019). The fact that water  
234 penetration occurred early during the development of these faults is attested by  
235 geochemical gradients continuous on distances reaching a few dozen of meters  
236 away from the faults (Rospabé et al., 2019). Concerning the lower temperature water  
237 circulation and greenschist facies alteration, the connection with former seafloor  
238 hydrothermal vents is attested by the occurrence of Fe, Ni and Cu sulfide  
239 mineralizations within these faults (Abily et al., 2011).

240 A recent survey showed that the Moho steepens in the massifs located close to the  
241 front of the Oman ophiolite. This unusual dipping is attributed to a ductile shear zone  
242 that was active in very high temperature conditions, close to the gabbro solidus



243 (Ceuleneer et al., 2020). The lower crustal cumulates are affected by plastic  
244 deformation on a thickness reaching 2 km and the along strike extent of the fault  
245 reaches 100 km subparallel to the paleo-ridge axis. The curvature of this mega-fault  
246 was continentward at the time of accretion. Away from the Moho, the decrease in the  
247 deformation intensity is correlated with a progressive flattening of the layering and  
248 foliation of the gabbros (listric fault kinematics). This major feature, of regional extent,  
249 is interpreted in terms of syn-accretion tectonics (Ceuleneer et al., 2020).

### 250 **3. Description of the seismic reflection profiles in the Enderby Basin**

251 Here we gather several examples from different seismic profiles to get an all-  
252 encompassing view of the typical seismic structures from the unambiguous oceanic  
253 crust in the northern part of the survey area to the ocean-continent transition zone to  
254 the south.

#### 255 *3.1. The northernmost part of the survey area*

256 In the northernmost end of the seismic sections we observe a well-defined oceanic  
257 crust characterized by: (1) a smooth flat and reflective top basement, (2) some short  
258 reflections in the shallowest part of the crust, (3) a transparent unit in the upper crust  
259 located above, (4) a more reflective lower crust, and (5) a set of horizontal reflectors  
260 at the base of the crust. We interpret this latter as the oceanic Moho, although  
261 various geological structures at the base of the crust may generate high-amplitude  
262 reflections (e.g. Collins et al., 1986). The thickness of the oceanic crust is usually 2-  
263 2.2 s TWTT corresponding to ~6.4-7 km (using Canales et al. (2003) relationship  
264 between crustal thickness and crustal reflection travel times), which is within the  
265 range of normal oceanic crust thicknesses ( $6 \pm 1$  km; e.g. Christeson et al., 2019). In

266 some places the crust is thicker than the normal oceanic crustal thickness. This is the  
267 case south of the Kerguelen plateau, where the crustal thickness reaches  
268 3.2 s TWTT (~10 km) but also at the western edge of the survey area where the crust  
269 reaches 2.5 s TWTT thickness (7.9 km at 60°E) (Supplementary Fig. S1). Both the  
270 flat top basement and the thickness of the oceanic crust argue for a formation at a  
271 magma-rich spreading center.

### 272 3.2. *Oblique reflectors in the oceanic crust away of the LOC (area 1)*

273 To the south, in area 1 (see Fig. 3), the most striking and intriguing features of the  
274 seismic reflection profiles are the numerous high-amplitude dipping reflectors in the  
275 lower oceanic crust. These deep reflectors occur along sections more than 150 km-  
276 long. They define a layer of almost constant thickness at the base of the oceanic  
277 crust (1.3 s TWTT on average that is ~4.6 km using a 7 km/s for the lower crust)  
278 (Electronic Supplement 1). A discontinuous upper horizontal reflector marks locally  
279 the top of this lower crustal layer (at 0.7-0.8 s TWTT depth below top basement that  
280 is ~1.9 km using a 5 km/s for the upper crust). At the base, the reflection Moho is well  
281 marked and defines an oceanic crust of normal thickness (~2-2.1 s TWTT on  
282 average) (Fig. 3).

283 The spacing between the deep reflectors is variable, reaching several kilometers.  
284 However, in sections where their distribution is more regular, the spacing is typically  
285 2 km. There, they are 5-6 km-long. Locally and rarely, they can reach 10 km-long  
286 where they reach the upper crust. While they dip either toward the continent or  
287 toward the ridge, they mostly occur as series of reflectors dipping in the same  
288 direction for several tens of kilometers before changing dip direction (Fig. 3). Such  
289 changes in the dip direction are not marked by any noticeable change neither at the

290 top basement nor at the reflection Moho. Multiple changes of dip direction also occur  
291 locally such as in profile GA-229/32, where lower crustal reflectors are crossing each  
292 other (Fig. 4a).

293 The deepest part of the lower crustal reflectors roots at the reflection Moho and their  
294 shallowest part flattens at the base of the transparent layer, giving them a general  
295 apparent sigmoidal shape (Fig. 4a and S2). Although the exact geometry of the  
296 reflectors is unknown (as we do not know the seismic velocity profile) we note that  
297 some of these reflectors merge with shallower horizontal ones (Supplementary  
298 Fig. S2). Rare deep reflectors are observed both in the crust and in the mantle as  
299 deep as 11.5 s TWTT (Fig. 5).

300 A few rising continentward dipping reflectors (CDRs) are observed in the upper crust  
301 but they do not reach the top basement. They are covered by long and continuous  
302 reflectors (reaching 4-5 km length), which are ubiquitous in the shallowest part of the  
303 crust (Figs. 4 and 5). The thickness of this set of shallow reflectors is on average  
304 0.5 s TWTT (1 km using a 4 km/s velocity for the uppermost crust) but may reach  
305 0.7-0.8 s TWTT locally (1.5 km at 4 km/s). These shallow reflectors mostly dip gently  
306 toward the ridge at the base and then become horizontal upward forming wedges, up  
307 to 10 km-long, in the uppermost part of the crust (Fig. 6). Within these wedges, the  
308 CDRs that rise up from the lower crust are discontinuous, distributed, short and  
309 almost perpendicular (on the time sections) to the shallow reflectors dipping toward  
310 the ridge. Because these shallow reflectors remind the seaward dipping reflectors  
311 (SDRs) observed at volcanic rifted margins, we have call them oceanic seaward  
312 dipping reflectors (OSDRs). Despite the occurrence of these OSDR wedges, the top  
313 basement is usually almost flat or very smooth and only very rare volcanoes or faults

314 can be inferred from the seismic reflection of the top basement (Supplementary  
315 Fig. S3).

### 316 *3.3. A specific network of lower crustal dipping reflectors close to the LOC (area 2)*

317 In area 2, close to the LOC (see Fig. 3), some profiles show a 20-40 km-long denser  
318 network of deep oceanward dipping reflectors (ODRs; 1 reflector every ~500 m),  
319 which systematically sole out onto the reflection Moho. This is particularly well  
320 observed in profile GA-229/32 (Figs. 3 and 7). There, a few ODRs reach the upper  
321 crust at the LOC and are progressively replaced by CDRs with higher reflectivity  
322 (Fig. 7). Short CDRs first observed in the mid-crust close to the LOC where the crust  
323 is thicker (2.4-2.8 s TWTT), are lengthening and deepening oceanwards. The CDRs  
324 finally reach the reflection Moho as the ODRs disappear at 30-40 km from the LOC.

325 This dense network of ODRs close to the LOC shows some variability from one  
326 profile to the other: e.g. profile GA-228/07 displays triangular-shaped areas with  
327 groups of deep reflectors dipping preferentially oceanwards or continentwards (Figs.  
328 3 and 4b). The top basement remains flat in area 2 except in profile GA-229/30.  
329 There, it is associated with a wedge of shallow reflectors in the uppermost crust  
330 beneath a small asymmetric basin at the seafloor (Supplementary Fig. S4). The  
331 ODRs systematically sole out onto the Moho, which is particularly well marked by a  
332 single continuous bright reflector (Figs. 3 and 7). In this area the Moho is nearly  
333 horizontal or slightly dipping continentwards, defining a thicker oceanic crust (~2.4 s  
334 TWTT) than in area 1 (Fig. 7). At the LOC the Moho branches out in a set of deep  
335 reflectors that shallow or deepen parallel to the ODRs and CDRs, respectively (Figs.  
336 7 and S5).

337 Above the termination of the reflection Moho, an oceanward step-up in the top  
338 basement is systematically observed (Fig. 7). It is 0.5 TWTT high (~1000m at 4 km/s  
339 for the uppermost crust) on average. Locally, within this basement high, 2-3 shallow  
340 reflectors are slightly dipping oceanwards and are recovered progressively by flatter  
341 lying reflectors in a fan shape structure, similarly to the OSDRs observed in area 1  
342 (Supplementary Fig. S5).

### 343 *3.4. The transitional domain to the south of the LOC (area 3)*

344 The area 3 (see Fig. 3) to the south of the LOC shows a progressively deeper and  
345 rougher top basement reaching >8 s TWTT. Some parts of the top basement still  
346 show high reflectivity, but the top basement becomes less reflective continentwards  
347 as intense normal faulting results in numerous rotated blocks (see Electronic  
348 Supplement 1). These normal faults, mainly dipping oceanwards, are rooting at a  
349 discontinuous horizontal reflector at ~1 s TWTT depth beneath the top basement.  
350 This reflector has been called UR (for upper reflector) by Gillard et al. (2019) in  
351 contrast to a discontinuous weaker lower reflector (LR) that is observed locally  
352 deeper at about 10 s TWTT. Some of these normal faults are sealed by horizontal  
353 shallow reflectors in the uppermost basement. Deep reflectors are also observed in  
354 area 3 (see Figs. 3 and Electronic Supplement 1). Close to the LOC, one of these  
355 reflectors is observed dipping continentwards as deep as 11 s TWTT (Fig. 3).

## 356 **4. Discussion**

### 357 *4.1. Synthesis of observations and first order interpretation away of the LOC*

358 Both the alternating series of ODRs and CDRs and the local crosscutting  
359 relationships between these reflectors contrast with earlier observations of lower

360 crustal reflectors dipping predominantly toward the paleo-ridge axis (e.g. Bécél et al.,  
361 2015; Ding et al., 2018; Reston et al., 1999). These new observations indicate that  
362 the ODRs and CDRs may locally be formed contemporaneously. We describe  
363 hereafter, from top to bottom of the oceanic crust, the various reflectors and infer  
364 their nature.

365 We interpret the CDRs that are locally reaching the upper crust as rotated dikes as  
366 they are distributed below, perpendicular to the OSDRs that we interpret as lava  
367 flows (Fig. 6). This systematic dipping of the shallowest lava flows toward the ridge  
368 and the rotation of the sheeted dike complex were described at fast-spreading  
369 centers by Karson (2002) on the basis of geological investigations of major fault  
370 scarps and DSDP/ODP Drill Holes. Evidence of shallow block rotation pre-dating the  
371 cessation of the magmatic activity along ridge parallel normal faults (i.e. with the  
372 same orientation as the deep faults) were also reported in Oman (MacLeod and  
373 Rothery, 1992).

374 The flat top basement above the wedges of OSDRs indicates that their formation  
375 occurred close enough to the paleo-ridge axis so that the latest lava flows within the  
376 neo-volcanic zone at the paleo-ridge axis sealed these wedges that were not  
377 deformed subsequently on the ridge flank. The neo-volcanic zone at fast-spreading  
378 ridges (zone of lava accumulation and dike intrusion at the ridge axis) is usually very  
379 narrow, few kilometers wide but the extent of these wedges within our study area  
380 shows that it may reach up to 10 km off-axis.

381 The rotation of the dikes and lava flows in the uppermost part of the crust must be  
382 accommodated below. The apparent sigmoid shape of the CDRs and ODRs and the  
383 local occurrence of a horizontal reflector marking the top of the layer of these dipping

384 reflectors suggest a decoupling layer there that could serve both for the CDRs and  
385 ODRs in the lower crust and for the rotated dikes above (Figs. 4 and S2). It is located  
386 at 0.7-0.8 s TWTT below the top basement (~1.9 km at 5 km/s), which corresponds  
387 to the depth of the magma chamber at fast-spreading ridges and therefore to the  
388 base of the dike complex. A decoupling level at the base of the dike complex was  
389 already suggested by Varga et al. (2004).

390 At the base of the crust, the rooting of the dipping reflectors onto the Moho indicates  
391 that this latter corresponds to another decoupling level (Figs. 3 and 7). The nearly  
392 horizontal reflection Moho together with the smooth top basement suggest that the  
393 processes forming these dipping reflectors are restricted to the lower crust as neither  
394 the base nor the top of the crust are affected. Considering that water is unlikely to  
395 penetrate down to 11.5 s TWTT deep within the mantle beneath a relatively thick  
396 magmatic crust, we suggest that the local occurrence of dipping reflectors in the  
397 mantle (Fig. 5) is best explained at depth by melt intrusions.

#### 398 *4.2. Synthesis of observations and first order interpretation close to the LOC*

399 The dense network of ODRs close to the LOC is not observed elsewhere in the  
400 Enderby Basin, suggesting that it is a specific feature at the onset of spreading. The  
401 thicker oceanic crust (~0.3 s TWTT more that is ~1 km thicker than normal) closer to  
402 the LOC than away shows that the magma supply was up to 15% larger at the onset  
403 of spreading than afterwards. This increase of the magma supply was sudden as  
404 suggested by the 1 km-high step-up in the top basement above the termination of the  
405 reflection Moho. We interpret the pile of shallow reflectors within this step-up as a  
406 thick wedge of lavas flowing toward the continent (Supplementary Fig. S5). The base  
407 of this wedge could then correspond to the paleo-top basement of a pre-oceanic

408 domain. The loading of volcanic material may have produced the flexure of this  
409 existing lithosphere.

410 The crustal thickness returned normal (2-2.1 s TWTT) after the onset of spreading. It  
411 decreased progressively as testified by a flat top basement and a ridgewards rising  
412 reflection Moho (see Fig. 3 and Electronic Supplement 1). There, starting from the  
413 LOC area, the ODRs become shorter, are progressively replaced by CDRs and  
414 finally terminate when the crustal thickness returns to normal. This suggests  
415 therefore a control of the occurrence ODRs vs. CDRs by the magma supply at the  
416 initial ridge.

417 This magma supply at the initial ridge may also display some variations. We have  
418 shown that locally the set of ODRs is replaced by CDRs just beneath a small  
419 asymmetric basin at the top basement and a wedge of lava flows underneath  
420 (Supplementary Fig. S4), which suggests a syn-tectonic volcanic building and thus a  
421 tectonic control. We therefore propose that there is a tradeoff between magma supply  
422 and extensional tectonics within the LOC area and that this tradeoff controlled the  
423 changes from ODRs to CDRs. For example, a basin at the top basement with a syn-  
424 tectonic wedge of lava flows underneath would indicate either less magma supply or  
425 a higher extensional rate that controls the termination of the set of ODRs. Alternating  
426 triangular-shaped areas with preferentially ODRs or CDRs (Fig. 3) would then show  
427 that this tradeoff could change over a short time scale. However, the nearly flat top  
428 basement above these dipping reflectors, shows that the proximity to the ridge axis  
429 may allow the equalization of the overall magma supply on a longer time scale by  
430 leveling the relief by the latest lava flows. Without well constrained spreading rates  
431 for the Enderby Basin, we cannot estimate these time scales.



432 Close to the LOC, the dense network of deep oceanward dipping reflectors that  
433 systematically sole out onto a sharp and highly reflective Moho suggests that the  
434 Moho behaved as a decoupling layer. Moreover, the branching out of the reflection  
435 Moho at its continentward termination, following either ODRs or CDRs that are also  
436 observed in the transitional domain to the south of the LOC (Supplementary Fig. S5),  
437 also suggests a tectonic control of the deepest structures of the lower oceanic crust  
438 at the onset of spreading. Therefore we propose that, although the initial spreading  
439 center can be largely seen as a magmatic system like the EPR (where plate  
440 separation is accommodated by ~2% tectonic strain; Escartín et al., 2007) relative to  
441 the adjacent hyper-extended and intruded continental lithosphere (Gillard et al.,  
442 2019), the newly formed oceanic crust may be deformed. The denser network of  
443 dipping reflectors close to the LOC would then suggest that this tectonic deformation  
444 is slightly more intense at the onset of spreading than later, once the oceanic ridge is  
445 more mature.

446 The progressively deeper and rougher top basement to the south of the LOC (Fig. 3)  
447 was interpreted as exhumed mantle with increasing magmatic addition toward the  
448 LOC (Gillard et al., 2019). This is also shown by normal faults that are sealed by lava  
449 flows close to the LOC but that offset the top basement far away from it. Such  
450 increasing magma volume from the continent toward the ocean with magma addition  
451 both on the top and within the basement together with complex magma-fault  
452 relationships have already been described in other magma-poor rifted margins  
453 (Gillard et al., 2017).

454 *4.3. How do observations in the Oman ophiolite help to understand the nature and*  
455 *the origin of the lower crustal dipping reflectors?*

456 Bécel et al. (2015) proposed that the lower crustal dipping reflections within the fast  
457 spread crust offshore Alaska arise from shear zones that form near the spreading  
458 center. They extensively discuss the physical properties of tectonic and magmatic  
459 features that could ultimately be imaged in the lower oceanic crust. They conclude  
460 that either solidified melt that was segregated within the shear structures,  
461 mylonitization along shear zones, crystal alignment and/or a combination of these  
462 processes may result in the bright dipping reflections (Bécel et al., 2015). These  
463 authors noted, however, that shear zones with scales similar to the lower crustal  
464 reflections they imaged have not been observed to date in ophiolites, with special  
465 reference to the Oman ophiolite supposed to have formed in a similar tectonic setting  
466 than their study area. As seen above (section 2.2), this assertion is contradicted by  
467 recent observations in Oman that led to revisiting previous interpretations.

468 Accordingly, we suggest that syn-magmatic normal faulting revealed by new  
469 observations in the Oman ophiolite may correspond to the lower crustal dipping  
470 reflectors described in this study. We note similarities with the geometry of the  
471 dipping reflectors in the oceanic crust. They both dip either ridgeward or  
472 continentward within the lower crust and root at the crust-mantle transition zone.  
473 They also both occur within the hot ridge axial zone as evidenced by the latest lava  
474 flows sealing the top basement that remains almost flat and undeformed. It is  
475 important to note that the overall internal deformation is quite variable in Oman,  
476 where we observed faults with small normal displacement and major shear zones  
477 with displacement reaching likely one or more kilometers. The thickness of these  
478 major shear zones may reach tens of meters and could thus be wide enough to be  
479 imaged by seismic reflection techniques. In Oman, the faults appear to be closer

480 spaced than on the seismic reflection profiles but this is likely a question of spatial  
481 resolution.

482 Following Bécél et al. (2015), we hypothesize that the bright reflections observed in  
483 our seismic data set might have a hybrid tectonic and magmatic origin. In Oman, both  
484 late magmatic intrusions and low-temperature water circulation occur within the syn-  
485 magmatic fault zones. The water introduction produced mineralogical reactions that  
486 were active down to greenschist facies and that are absent from gabbroic cumulates  
487 located away of the fault zone. We therefore suggest that these lithological  
488 modifications, restricted to the vicinity of syn-magmatic fault zones, may result in  
489 velocity and density contrasts sufficient enough to create an impedance contrast at  
490 the location of these faults. We further speculate that these processes could thus  
491 explain the brightness of the dipping reflectors observed in our seismic reflection  
492 profiles. Another possible interpretation might be looked for in the  
493 anisotropy/polarizing effects related to the igneous layering. Away from faults the  
494 bedding is quite regular but this regularity is totally lost in the vicinity (hundreds of  
495 meters) of syn-magmatic faults, as illustrated by our observations in Oman. This  
496 sudden lack of regularity (which goes along with an increase in alteration) might  
497 induce contrasts in the seismic wave propagation and be imaged as a reflector. More  
498 work is needed to reinforce the comparison between lower crustal dipping reflectors  
499 and syn-magmatic faults.

#### 500 *4.4. Toward a more complex model of magmatic accretion*

501 Summing up our observations of lower crustal dipping reflectors in the Enderby Basin  
502 and their comparison with syn-magmatic and high temperature ductile faults  
503 observed in the Oman ophiolite suggest that internal sub-axial deformation processes

504 are more complicated than those shown in most current models of mid-ocean ridges.  
505 As a matter of fact, one of the main point revealed by studies in the Oman ophiolite is  
506 that very high temperature (up to syn-magmatic), high temperature (sub-solidus  
507 plastic deformation) and low temperature (brittle) deformation may coexist along the  
508 same fault over distances of several hundred meters at Moho depth. This huge  
509 temperature gradient likely results from the juxtaposition and interaction between  
510 crystallizing magmas and hydrothermal fluids induced by the episodic nucleation of  
511 faults in a context of continuous spreading (Rospabé et al., 2019).

512 A clear effect of crustal deformation is the rotation of originally horizontal lava flows  
513 and originally steeply dipping dikes to ridgeward and outward-dipping orientations,  
514 respectively (Fig. 8). These rotations are evident in outcrops of the upper crust at  
515 fast-spreading centers and in the Oman ophiolite (MacLeod and Rothery, 1992;  
516 Pallister and Hopson, 1981). Axial loading of lavas is generally considered to be the  
517 driving mechanism for this asymmetrical, subsidence of upper crustal units (Dewey  
518 and Kidd, 1977). This sub-axial subsidence is rapid beneath the ridge axis and  
519 decreases up to the edge of the active volcanic zone, a few kilometers for fast-  
520 spreading ridges (Karson, 2002). However, our observations show that, within this  
521 axial zone, deformation may affect the underlying deeper gabbroic units as well.

522 Flexure of the upper crustal units in the brittle regime creates accommodation space.  
523 At deeper levels, we suggest that early, syn- to sub-magmatic deformation as well as  
524 later brittle deformation is accommodated by syn-magmatic faulting as evidenced by  
525 the network of the dipping reflectors in the lower oceanic crust (Fig. 8). We infer a  
526 decoupling level at the base of the dikes, as already suggested by Karson et al.  
527 (2002) and Varga et al. (2004) for the fast-spreading East Pacific Rise, which results

528 in a partitioning of the deformation between the upper and lower crust. Gabbroic sills  
529 may have been emplaced beneath the dike complex and not have fully crystallized  
530 when the subsidence and deformation occurred in overlying units (Karson et al.,  
531 2015; Yoshinobu and Harper, 2004).

532 Differences in melt supply along the axis of the fast-spreading East Pacific Rise have  
533 been mapped by seismic reflection experiments with pure melt zones, inferred to  
534 correspond to regions of fresh magma supply from the mantle asthenosphere, and  
535 mush zones, inferred to have undergone cooling and crystallization and to be more  
536 evolved (Singh et al., 1998). Significant temporal heterogeneities in the magma  
537 plumbing system beneath this ridge were also suggested to account for the observed  
538 differences between the geochemistry and petrology of the plutonic rocks recovered  
539 from Hess Deep and Pito Deep (Perk et al., 2007). We suggest that such short  
540 timescale changes of magma supply and subsequent thermal structure may influence  
541 the lower crustal sub-axial deformation. The predominance of ODRs in the lower  
542 crust during high magma delivery at the onset of seafloor spreading suggests that  
543 syn-magmatic faults rooting at the Moho are a particularly efficient way for  
544 accommodating space at the base of the crust in the hot axial zone in addition to new  
545 melt intrusions (Fig. 8). The occurrence of CDRs on top of the ODRs and their  
546 progressive lengthening and deepening up to the complete replacement of the ODRs  
547 while the magma supply turns back to normal would then suggest that CDRs rather  
548 result from the compaction and subsidence of the lower crust as it cools. This mode  
549 of spreading with somewhat less magma supply is more likely to trigger vertical mass  
550 transport. Some of the CDRs that reach locally the upper crust may thus indicate an  
551 episodic coupling of the upper and lower crust when the magma budget/pressure is  
552 lower. Both ODRs and CDRs are thus contemporaneous and participate to the

553 hydrothermal cooling of the crust but their extent could be related to the tradeoff  
554 between magma supply and tectonic deformation. This latter is probably relatively  
555 constant at the mature spreading center but may be variable at the onset of  
556 spreading.

## 557 **5. Conclusions**

558 The main results of our interpretation of high-quality seismic reflection profiles across  
559 the ocean-continent transition in the Enderby Basin, between the Kerguelen Plateau  
560 and the Antarctic margin, are as follows:

- 561 1. While lower crustal events dipping toward the paleo-ridge axis were  
562 predominantly described until now, we identified numerous both rideward and  
563 continentward dipping high-amplitude dipping reflectors in the lower oceanic  
564 crust;
- 565 2. We suggest that these lower crustal dipping reflectors correspond to syn-  
566 magmatic faults previously described in the Oman ophiolite;
- 567 3. Evidence for such syn-accretion tectonism at depth together with the  
568 systematic rotation of originally horizontal lava flows pre-dating the cessation  
569 of the magmatic activity argue for deformation within the axial zone of  
570 magmatic spreading centers.

## 571 **Acknowledgements**

572 Seismic sections of the AGSO surveys GA-228 and GA-229 have been provided by  
573 Geoscience Australia and are published with the permission of Geoscience Australia.  
574 These seismic data are freely available from Geoscience Australia upon request. We  
575 would like to acknowledge the support and kindness of Aaron Rockey and the other

576 employees of Geoscience Australia. Gravity grid of Sandwell et al. (2014) is freely  
577 available from the website of the UCSD ([topex.ucsd.edu/cgi-bin/get\\_data.cgi](http://topex.ucsd.edu/cgi-bin/get_data.cgi)). We  
578 thank Alexander Golynsky for providing the magnetic grid of the Antarctic margin. We  
579 also gratefully acknowledge Jeffrey Karson and the Editor, Jean-Philippe Avouac, for  
580 their review and helpful comments. Support was provided by the French Institut  
581 National des Sciences de l'Univers INSU-CNRS.

582 **Figure captions:**

583 Fig. 1: Map of the eastern Enderby Basin. The background image is the free air  
584 gravity anomaly grid derived from satellite altimetry data (Sandwell et al., 2014). The  
585 black dashed line indicates the landward edge of the oceanic crust (LOC) after Gaina  
586 et al. (2007). The white dashed line indicates the presumed extinct ridge axis after  
587 Gibbons et al. (2013). The squares show the magnetic anomaly picks from Gibbons  
588 et al. (2013). The black lines indicate the seismic profiles from Geoscience Australia  
589 used in this paper. Their thickened and dashed parts correspond to the sections  
590 shown in Fig. 3. The white star indicates the location of Fig. 6. Ker., Kerguelen Island;  
591 CIR, Central Indian Ridge; SEIR, Southeast Indian Ridge; SWIR, Southwest Indian  
592 Ridge.

593 Fig. 2: Evidence of syn-magmatic normal faulting and block rotation at Moho level in  
594 the Oman ophiolite, Maqsad area (see also Abily et al. (2011)). (a) Simplistic  
595 sketches illustrating the possible context of acquisition of the structures observed in  
596 the field (left) and the evolution in the conditions of deformation along the fault (right).  
597 (b) Main structural elements observed on this outcrop: magmatic layering (thin black  
598 lines); ductile faults (thick black lines and arrows), deformed crystal mush layer (red  
599 symbols). (c) Closer view on the zone of former crystal mush with complex modal

600 layering induced by crystal sorting and melt injection during viscous deformation. (d)  
601 Detail on a ptygmatic fold and on the upper horizon of pegmatite (former melt layer  
602 that made possible the mechanical decoupling between the tilted blocks of layered  
603 cumulates and the overlying cumulates).

604 Fig. 3: Line drawing of 4 seismic profiles across the landward edge of the oceanic  
605 crust (LOC indicated by the green band). Blue lines indicate oceanward dipping  
606 reflectors (ODRs); red ones indicate continentward dipping reflectors (CDRs); yellow  
607 ones show nearly horizontal reflectors and orange ones at the top basement indicate  
608 oceanic seawards dipping reflectors (OSDRs). The thick orange lines at the bottom of  
609 the crust show the reflection Moho and the black lines beneath it show where the  
610 Moho is continuous and highly reflective. The blue band indicates the rideward end  
611 of the dense network of ODRs occurring close to the LOC. Vertical exaggeration is  
612 approximately x2. Uninterpreted and interpreted versions of profiles 229/32 with no  
613 vertical exaggeration are shown in the Electronic Supplement 1.

614 Fig. 4: Examples of dipping reflectors crossing each other (a: profile 229/32 and b:  
615 profile 228/07) defining a layer of almost constant thickness at the base of the  
616 oceanic crust. The reflection Moho is well marked almost all along the bottom of the  
617 layer. See figure caption and location in Fig. 3. Approximately no vertical  
618 exaggeration. Copyright Commonwealth of Australia (Geoscience Australia).

619 Fig. 5: Example of reflectors that are observed both in the crust and in the mantle as  
620 deep as 11.5 s TWTT (line 229/33). Note some rare examples of dipping reflectors  
621 that are shallowing but do not reach the top basement as they are covered by long  
622 and continuous reflectors. See figure caption and location in Fig. 3. Approximately no  
623 vertical exaggeration. Copyright Commonwealth of Australia (Geoscience Australia).



624 Fig. 6: Example of oceanic seawards dipping reflectors (OSDRs) forming up to  
625 ~10 km-long wedges in the uppermost part of the crust (profile 229/31). Same figure  
626 caption as Fig. 3. See location in Fig. 1. Approximately no vertical exaggeration.  
627 Copyright Commonwealth of Australia (Geoscience Australia).

628 Fig. 7: Denser network of oceanward dipping reflectors (ODRs) and continentward  
629 dipping reflectors (CDRs) (1 reflector every ~500 m) close to the landward edge of  
630 the oceanic crust (profile 229/32). Vertical exaggeration is approximately 2x. See  
631 figure caption and location in Fig. 3. Copyright Commonwealth of Australia  
632 (Geoscience Australia).

633 Fig. 8: Cartoon of the structure of the oceanic ridge showing the formation of dipping  
634 reflectors by sub-axial deformation (CDR, continentwards dipping reflectors; ODR,  
635 oceanwards dipping reflectors; OSDR, oceanic seaward dipping reflectors). Oblique  
636 reflectors in the lower crust are syn-magmatic faults. Isotherms (dotted blue lines)  
637 and hydrothermal circulation paths (green line) are schematic. AML: axial melt lens.  
638 No vertical exaggeration.

## 639 REFERENCES CITED

640 Abily, B., Ceuleneer, G., and Launeau, P., 2011, Synmagmatic normal faulting in the  
641 lower oceanic crust: Evidence from the Oman ophiolite: *Geology*, v. 39, p.  
642 391-394, doi:10.1130/g31652.1.

643 Amri, I., Benoit, M., and Ceulener, G., 1996, Tectonic setting for the genesis of  
644 oceanic plagiogranites: evidence from a paleo-spreading structure in the  
645 Oman ophiolite: *Earth and Planetary Science Letters*, v. 139, p. 177-194.

646 Bécél, A., Shillington, D.J., Nedimović, M.R., Webb, S.C., and Kuehn, H., 2015,  
647 Origin of dipping structures in fast-spreading oceanic lower crust offshore  
648 Alaska imaged by multichannel seismic data: *Earth and Planetary Science*  
649 *Letters*, v. 424, p. 26-37, doi:<http://dx.doi.org/10.1016/j.epsl.2015.05.016>.

650 Boudier, F., Bouchez, J.-L., Nicolas, A., Cannat, M., Ceuleneer, G., Misseri, M., and  
651 Montigny, R., 1985, Kinematics of oceanic thrusting in the Oman ophiolite:  
652 model of plate convergence: *Earth and Planetary Science Letters*, v. 75, p.  
653 215-222.

654 Boudier, F., Ceuleneer, G., and Nicolas, A., 1988, Shear zones, thrusts and related  
655 magmatism in the Oman ophiolite: Initiation of thrusting on an oceanic ridge:  
656 *Tectonophysics*, v. 151, p. 275-296, doi:[https://doi.org/10.1016/0040-](https://doi.org/10.1016/0040-1951(88)90249-1)  
657 [1951\(88\)90249-1](https://doi.org/10.1016/0040-1951(88)90249-1).

658 Brown, T.C., Cheadle, M.J., John, B.E., Coogan, L.A., Gee, J.S., Karson, J.A., and  
659 Swapp, S.M., 2019, Textural Character of Gabbroic Rocks from Pito Deep: a  
660 Record of Magmatic Processes and the Genesis of the Upper Plutonic Crust  
661 at Fast-Spreading Mid-Ocean Ridges: *Journal of Petrology*, v. 60, p. 997-  
662 1026, doi:[10.1093/petrology/egz022](https://doi.org/10.1093/petrology/egz022).

663 Canales, J.P., Detrick, R.S., Toomey, D.R., and Wilcock, S.D., 2003, Segment-scale  
664 variations in crustal structure of 150- to 300-k.y.-Old fast spreading oceanic  
665 crust (East Pacific Rise, 8°15'N-10°15'N from wide-angle seismic refraction  
666 profiles: *Geophysical Journal International*, v. 152, p. 766-794.

667 Ceuleneer, G., Abily, B., Python, M., Kaczmarek, M.-A., Rospabé, M., Grégoire, M.,  
668 Benoit, M., and le Sueur, E., 2020, Crustal accretion along a giant high-

669 temperature normal fault at the front of the Oman ophiolite: evidence from the  
670 Bahla and some other massifs, International Conference on Ophiolites and  
671 the Oceanic Lithosphere: Results of the Oman Drilling Project and Related  
672 Research: Muscat, Sultanate of Oman, Sultan Qaboos University, p. 3.

673 Ceuleneer, G., Monnereau, M., and Amri, I., 1996, Thermal structure of a fossil  
674 mantle diapir inferred from the distribution of mafic cumulates: *Nature*, v. 379,  
675 p. 149-153, doi:10.1038/379149a0.

676 Christeson, G.L., Goff, J.A., and Reece, R.S., 2019, Synthesis of Oceanic Crustal  
677 Structure from Two-Dimensional Seismic Profiles: *Reviews of Geophysics*, v.  
678 57, p. 504-529, doi:10.1029/2019rg000641.

679 Collins, J.A., Brocher, T.M., and Karson, J.A., 1986, Two-dimensional seismic  
680 reflection modeling of the inferred fossil oceanic crust/mantle transition in the  
681 Bay of Islands Ophiolite: *Journal of Geophysical Research: Solid Earth*, v. 91,  
682 p. 12520-12538, doi:10.1029/JB091iB12p12520.

683 Constantin, M., Hékinian, R., Bideau, D., and Hébert, R.j., 1996, Construction of the  
684 oceanic lithosphere by magmatic intrusions: Petrological evidence from  
685 plutonic rocks formed along the fast-spreading East Pacific Rise: *Geology*, v.  
686 24, p. 731-734, doi:10.1130/0091-7613(1996)024<0731:cotolb>2.3.co;2.

687 Crawford, W.C., and Webb, S.C., 2002, Variations in the distribution of magma in the  
688 lower crust and at the Moho beneath the East Pacific Rise at 9°-10°N: *Earth  
689 and Planetary Science Letters*, v. 202, p. 117-130.

690 Davis, J.K., Lawver, L.A., Norton, I.O., Dalziel, I.W.D., and Gahagan, L.M., 2018, The  
691 crustal structure of the Enderby Basin, East Antarctica: *Marine Geophysical*  
692 *Research*, v. 40, p. 1-16, doi:10.1007/s11001-018-9356-5.

693 Detrick, R.S., Buhl, P., Vera, E.E., Mutter, J.C., Orcutt, J.A., Madsen, J.A., and  
694 Brocher, T.M., 1987, Multi-channel seismic imaging of a crustal magma  
695 chamber along the East Pacific Rise: *Nature*, v. 326, p. 35-41.

696 Dewey, J.F., and Kidd, W.S.F., 1977, Geometry of plate accretion: *GSA Bulletin*, v.  
697 88, p. 960-968, doi:10.1130/0016-7606(1977)88<960:gopa>2.0.co;2.

698 Dijkstra, A.H., Drury, M.R., and Frijhoff, R.M., 2002, Microstructures and lattices in  
699 the Hilti mantle section (Oman Ophiolite): Evidence for shear localization and  
700 melt weakening in the crust mantle transition zone?: *Journal of Geophysical*  
701 *Research*, v. 107, p. 10.1029/2001JB000458.

702 Ding, W., Sun, Z., Dadd, K., Fang, Y., and Li, J., 2018, Structures within the oceanic  
703 crust of the central South China Sea basin and their implications for oceanic  
704 accretionary processes: *Earth and Planetary Science Letters*, v. 488, p. 115-  
705 125, doi:https://doi.org/10.1016/j.epsl.2018.02.011.

706 Escartín, J., Soule, S.A., Fornari, D.J., Tivey, M.A., Schouten, H., and Perfit, M.R.,  
707 2007, Interplay between faults and lava flows in construction of the upper  
708 oceanic crust: The East Pacific Rise crest 9°25'–9°58'N: *Geochemistry,*  
709 *Geophysics, Geosystems*, v. 8, doi:10.1029/2006gc001399.

710 Gaina, C., Muller, R.D., Brown, B., Ishihara, T., and Ivanov, S., 2007, Breakup and  
711 early seafloor spreading between India and Antarctica: *Geophysical Journal*  
712 *International*, v. 170, p. 151-169, doi:doi:10.1111/j.1365-246X.2007.03450.x.

713 Gibbons, A.D., Whittaker, J.M., and Müller, R.D., 2013, The breakup of East  
714 Gondwana: Assimilating constraints from Cretaceous ocean basins around  
715 India into a best-fit tectonic model: *Journal of Geophysical Research: Solid*  
716 *Earth*, v. 118, p. 808-822, doi:10.1002/jgrb.50079.

717 Gillard, M., Sauter, D., Tugend, J., Tomasi, S., Epin, M.-E., and Manatschal, G.,  
718 2017, Birth of an oceanic spreading center at a magma-poor rift system:  
719 *Scientific Reports*, v. 7, p. 15072, doi:10.1038/s41598-017-15522-2.

720 Gillard, M., Tugend, J., Müntener, O., Manatschal, G., Karner, G.D., Autin, J., Sauter,  
721 D., Figueredo, P.H., and Ulrich, M., 2019, The role of serpentinization and  
722 magmatism in the formation of decoupling interfaces at magma-poor rifted  
723 margins: *Earth-Science Reviews*, v. 196, p. 102882,  
724 doi:<https://doi.org/10.1016/j.earscirev.2019.102882>.

725 Gillis, K.M., Snow, J.E., Klaus, A., Abe, N., Adriaio, A.B., Akizawa, N., Ceuleneer, G.,  
726 Cheadle, M.J., Faak, K., Falloon, T.J., Friedman, S.A., Godard, M., Guerin,  
727 G., Harigane, Y., Horst, A.J., Hoshide, T., Ildefonse, B., Jean, M.M., John,  
728 B.E., Koepke, J., Machi, S., Maeda, J., Marks, N.E., McCaig, A.M., Meyer,  
729 R., Morris, A., Nozaka, T., Python, M., Saha, A., and Wintsch, R.P., 2014,  
730 Primitive layered gabbros from fast-spreading lower oceanic crust: *Nature*, v.  
731 505, p. 204-207, doi:10.1038/nature12778.

732 Golynsky, A.V., Ivanov, S.V., Kazankov, A.J., Jokat, W., Masolov, V.N., and von  
733 Frese, R.R.B., 2013, New continental margin magnetic anomalies of East  
734 Antarctica: *Tectonophysics*, v. 585, p. 172-184,  
735 doi:<http://dx.doi.org/10.1016/j.tecto.2012.06.043>.

736 Jokat, W., Nogi, Y., and Leinweber, V., 2010, New aeromagnetic data from the  
737 western Enderby Basin and consequences for Antarctic-India break-up:  
738 *Geophysical Research Letters*, v. 37, p. L21311, doi:10.1029/2010gl045117.

739 Jousselin, D., and Nicolas, A., 2000, The Moho transition in the Oman ophiolite -  
740 relation with wherlites in the crust and dunites in the mantle: *Marine*  
741 *Geophysical Researches*, v. 21, p. 229-241.

742 Jousselin, D., Nicolas, A., and Boudier, F., 1998, Detailed mapping of a mantle diapir  
743 below a paleo-spreading center in the Oman ophiolite: *Journal of*  
744 *Geophysical Research: Solid Earth*, v. 103, p. 18153-18170,  
745 doi:10.1029/98jb01493.

746 Karson, J.A., 2002, Geologic Structure of uppermost oceanic crust created at fast to  
747 intermediate-rate spreading centers: *Annual Reviews of Earth and Planetary*  
748 *Sciences*, v. 30, p. 10.1146/annurev.earth.30.091201.141132.

749 Karson, J.A., Kelley, D.S., Fornari, D.J., Perfit, M.R., and Shank, T.M., 2015,  
750 *Discovering the Deep: A Photographic Atlas of the Seafloor and Ocean*  
751 *Crust*, Cambridge University Press, 413 p.

752 Karson, J.A., Klein, E.M., Hurst, S.D., Lee, C.D., Rivizzigno, P.A., Curewitz, D.,  
753 Morris, A.R., and Party, H.D.S., 2002, Structure of uppermost fast-spreading

754 oceanic crust exposed at the Hess Deep Rift: Implications for subaxial  
755 processes at the East Pacific Rise: *Geochemistry, Geophysics, Geosystems*,  
756 v. 3, p. 2001GC000155.

757 Kelemen, P.B., Koga, K., and Shimizu, N., 1997, *Geochemistry of gabbro sills in the*  
758 *crust/mantle transition zone of the Oman ophiolite: Implications for the origin*  
759 *of the oceanic lower crust: Earth and Planetary Science Letters*, v. 146, p.  
760 475-488.

761 MacLeod, C.J., Johan Lissenberg, C., and Bibby, L.E., 2013, "Moist MORB" axial  
762 magmatism in the Oman ophiolite: The evidence against a mid-ocean ridge  
763 origin: *Geology*, v. 41, p. 459-462, doi:10.1130/g33904.1.

764 MacLeod, C.J., and Rothery, D.A., 1992, Ridge axial segmentation in the Oman  
765 ophiolite: evidence from along-strike variations in the sheeted dyke complex,  
766 in Parson, L.M., Murton, B.J., and Browning, P., eds., *Ophiolites and their*  
767 *modern oceanic analogues*, Volume 60: Geological Society Special  
768 Publication, Geological Society, p. 39-63.

769 MacLeod, S.J., Williams, S.E., Matthews, K.J., Müller, R.D., and Qin, X., 2017, A  
770 global review and digital database of large-scale extinct spreading centers:  
771 *Geosphere*, v. 13, p. 911-949, doi:10.1130/ges01379.1.

772 Marjanovic, M., Carbotte, S.M., Carton, H., Nedimovic, M.R., Mutter, J.C., and  
773 Canales, J.P., 2014, A multi-sill magma plumbing system beneath the axis of  
774 the East Pacific Rise: *Nature Geosci*, v. 7, p. 825-829,  
775 doi:10.1038/ngeo2272.

776 McElhinny, M.W., 1970, Formation of the Indian Ocean: *Nature*, v. 228, p. 977-979,  
777 doi:10.1038/228977a0.

778 Nicolas, A., and Boudier, F., 2015, Structural contribution from the Oman ophiolite to  
779 processes of crustal accretion at the East Pacific Rise: *Terra Nova*, v. 27, p.  
780 77-96, doi:10.1111/ter.12137.

781 Pallister, J.S., and Hopson, C., 1981, Samail Ophiolite plutonic suite: Field relations,  
782 phase variation, cryptic variation and layering, and a model of a spreading  
783 ridge magma chamber: *Journal of Geophysical Research*, v. 86, p. 2593-  
784 2644.

785 Perk, N.W., Coogan, L.A., Karson, J.A., Klein, E.M., and Hanna, H.D., 2007,  
786 Petrology and geochemistry of primitive lower oceanic crust from Pito Deep:  
787 implications for the accretion of the lower crust at the Southern East Pacific  
788 Rise: *Contributions to Mineralogy and Petrology*, v. 154, p. 575-590,  
789 doi:10.1007/s00410-007-0210-z.

790 Quick, J.E., and Delinger, R.P., 1993, Ductile deformation and the origin of layered  
791 gabbro in ophiolites: *Journal of Geophysical Research*, v. 98, p. 14015-  
792 14027.

793 Reston, T.J., Ranero, C.R., and Belykh, I., 1999, The structure of Cretaceous  
794 oceanic crust of the NW Pacific: Constraints on processes at fast spreading  
795 centers: *Journal of Geophysical Research: Solid Earth*, v. 104, p. 629-644,  
796 doi:10.1029/98jb02640.



797 Rioux, M., Bowring, S., Kelemen, P., Gordon, S., Dudás, F., and Miller, R., 2012,  
798 Rapid crustal accretion and magma assimilation in the Oman-U.A.E.  
799 ophiolite: High precision U-Pb zircon geochronology of the gabbroic crust:  
800 Journal of Geophysical Research: Solid Earth, v. 117,  
801 doi:10.1029/2012jb009273.

802 Rospabé, M., Benoit, M., Ceuleneer, G., Kaczmarek, M.-A., and Hodel, F., 2019, Melt  
803 hybridization and metasomatism triggered by syn-magmatic faults within the  
804 Oman ophiolite: A clue to understand the genesis of the dunitic mantle-crust  
805 transition zone: Earth and Planetary Science Letters, v. 516, p. 108-121,  
806 doi:<https://doi.org/10.1016/j.epsl.2019.04.004>.

807 Rospabé, M., Ceuleneer, G., Benoit, M., Abily, B., and Pinet, P., 2017, Origin of the  
808 dunitic mantle-crust transition zone in the Oman ophiolite: The interplay  
809 between percolating magmas and high-temperature hydrous fluids: Geology,  
810 v. 45, p. 471-474, doi:10.1130/g38778.1.

811 Sandwell, D.T., Müller, R.D., Smith, W.H.F., Garcia, E., and Francis, R., 2014, New  
812 global marine gravity model from CryoSat-2 and Jason-1 reveals buried  
813 tectonic structure: Science, v. 346, p. 65-67, doi:10.1126/science.1258213.

814 Singh, S.C., Kent, G.M., Collier, J.S., Harding, A.J., and Orcutt, J.O., 1998, Melt to  
815 mush variations in crustal magma properties along the ridge crest at the  
816 southern East Pacific Rise: Nature, v. 394, p. 874-878.

817 Sinton, J.M., and Dietrick, R.S., 1992, Mid-ocean Ridge magma chambers: J.  
818 Geophys. Res., v. 97, p. 197-216.

819 Stagg, H.M.J., Colwel, J.B., Direen, N.G., O'Brien, P.E., Bernardel, G., Borissova, I.,  
820 Brown, B.J., and Ishirara, T., 2005, Geology of the Continental Margin of  
821 Enderby and Mac. Robertson Lands, East Antarctica: Insights from a  
822 Regional Data Set: Marine Geophysical Researches, v. 25, p. 183-219,  
823 doi:10.1007/s11001-005-1316-1.

824 Toomey, D.R., Purdy, G.M., Solomon, S.C., and Wilcock, W.S.D., 1990, The three-  
825 dimensional seismic velocity structure of the East Pacific Rise near latitude  
826 9°30' N: Nature, v. 347, p. p. 639-645.

827 Varga, R.J., Karson, J.A., and Gee, J.S., 2004, Paleomagnetic constraints on  
828 deformation models for uppermost oceanic crust exposed at the Hess Deep  
829 Rift: Implications for axial processes at the East Pacific Rise: Journal of  
830 Geophysical Research: Solid Earth, v. 109, doi:doi:10.1029/2003JB002486.

831 Yoshinobu, A.S., and Harper, G.D., 2004, Hypersolidus deformation in the lower  
832 crust of the Josephine ophiolite: evidence for kinematic decoupling between  
833 the upper and lower oceanic crust: Journal of Structural Geology, v. 26, p.  
834 163-175.

835 Zihlmann, B., Müller, S., Coggon, R.M., Koepke, J., Garbe-Schönberg, D., and  
836 Teagle, D.A.H., 2018, Hydrothermal fault zones in the lower oceanic crust:  
837 An example from Wadi Gideah, Samail ophiolite, Oman: Lithos, v. 323, p.  
838 103-124, doi:https://doi.org/10.1016/j.lithos.2018.09.008.

839

Fig. 1

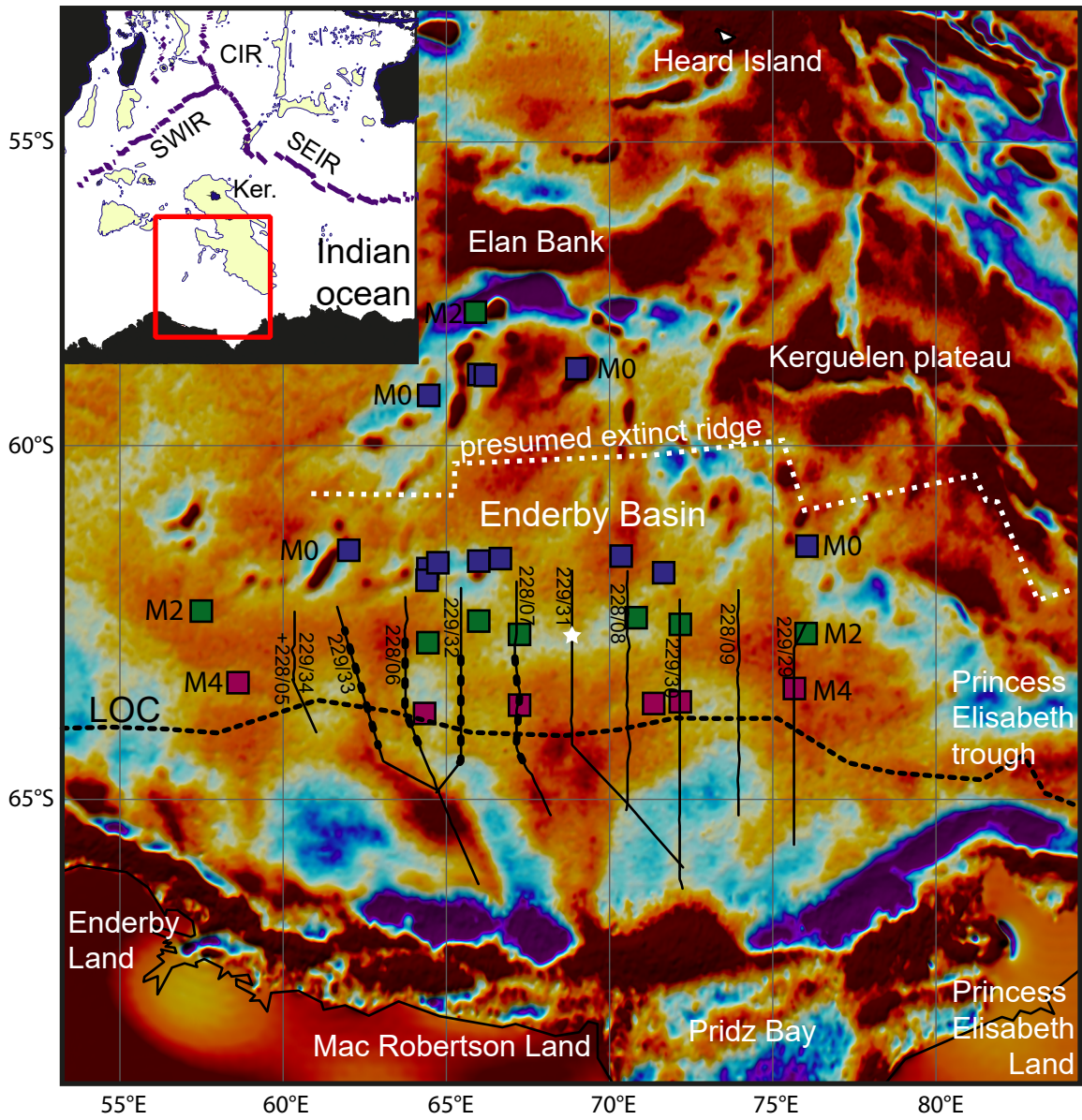




Fig. 2

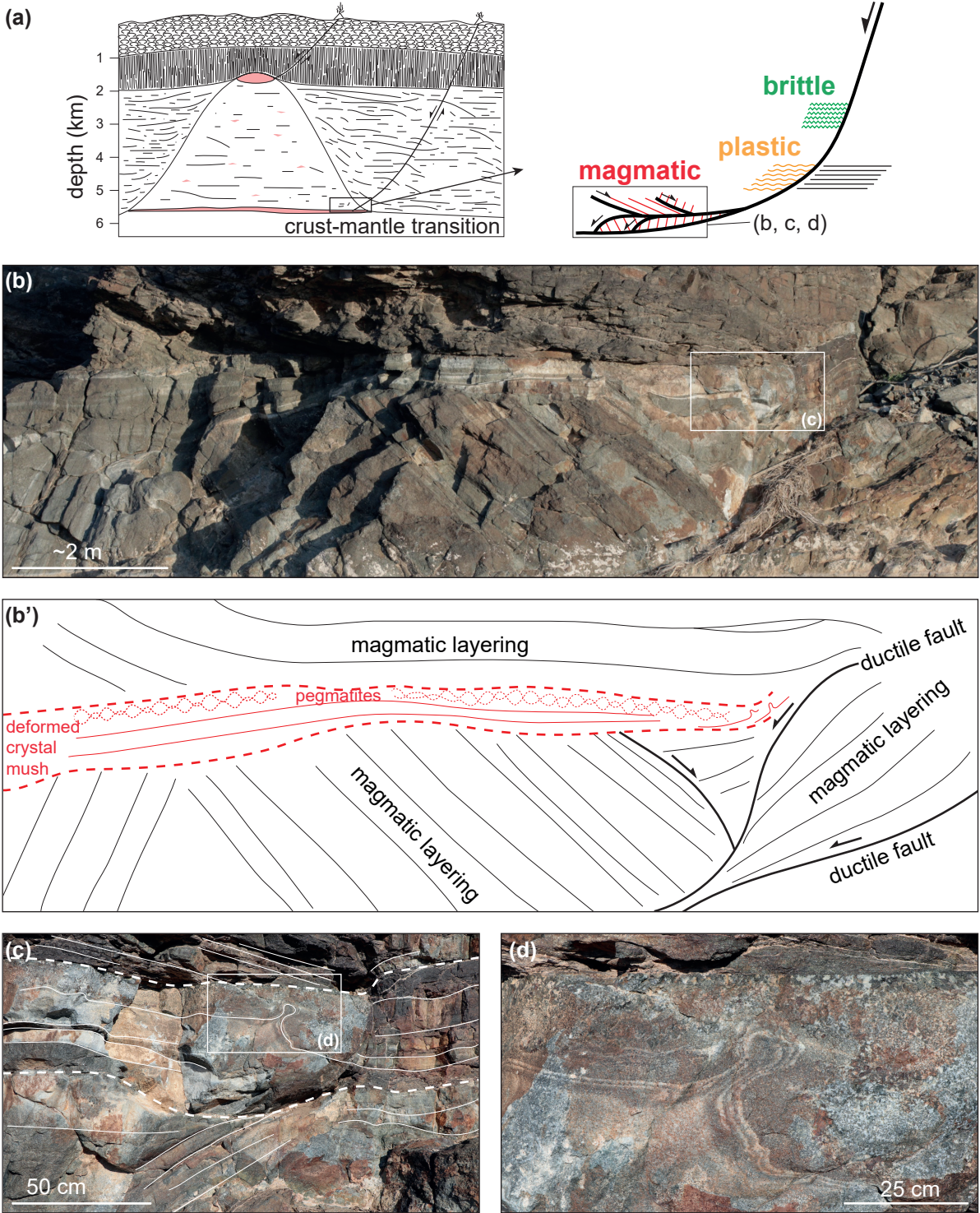


Fig. 3

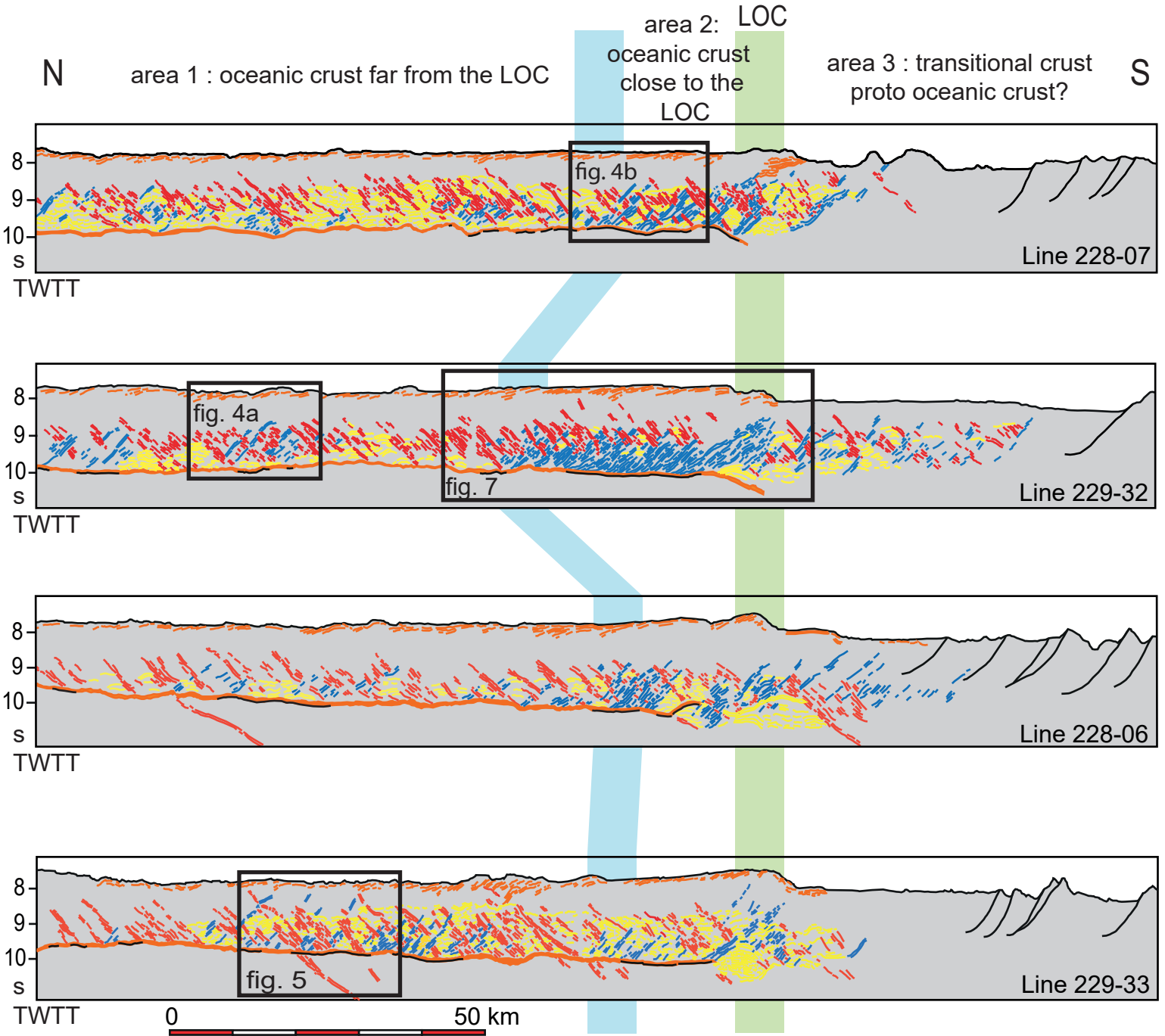




FIG. 4

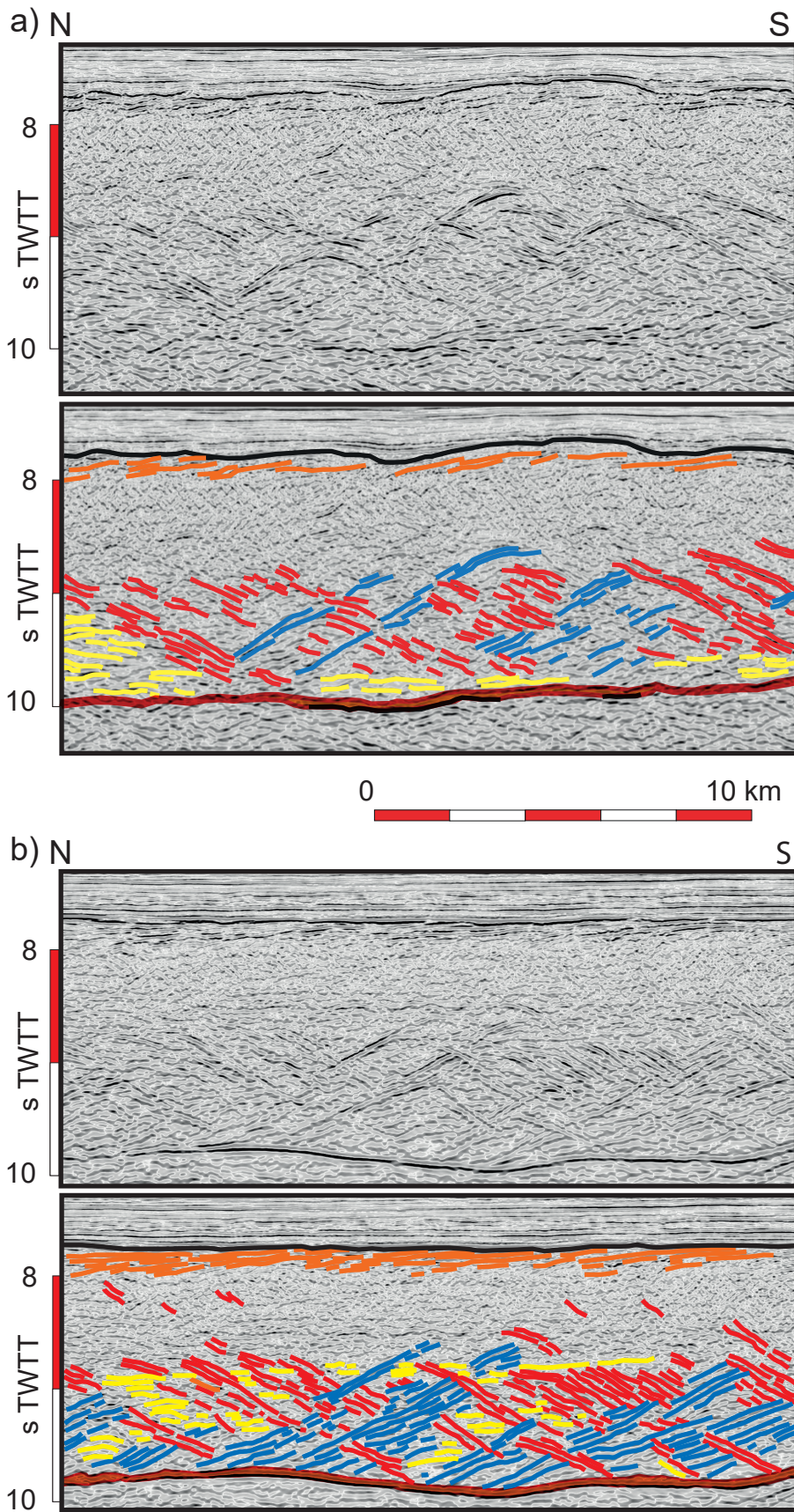




FIG. 5

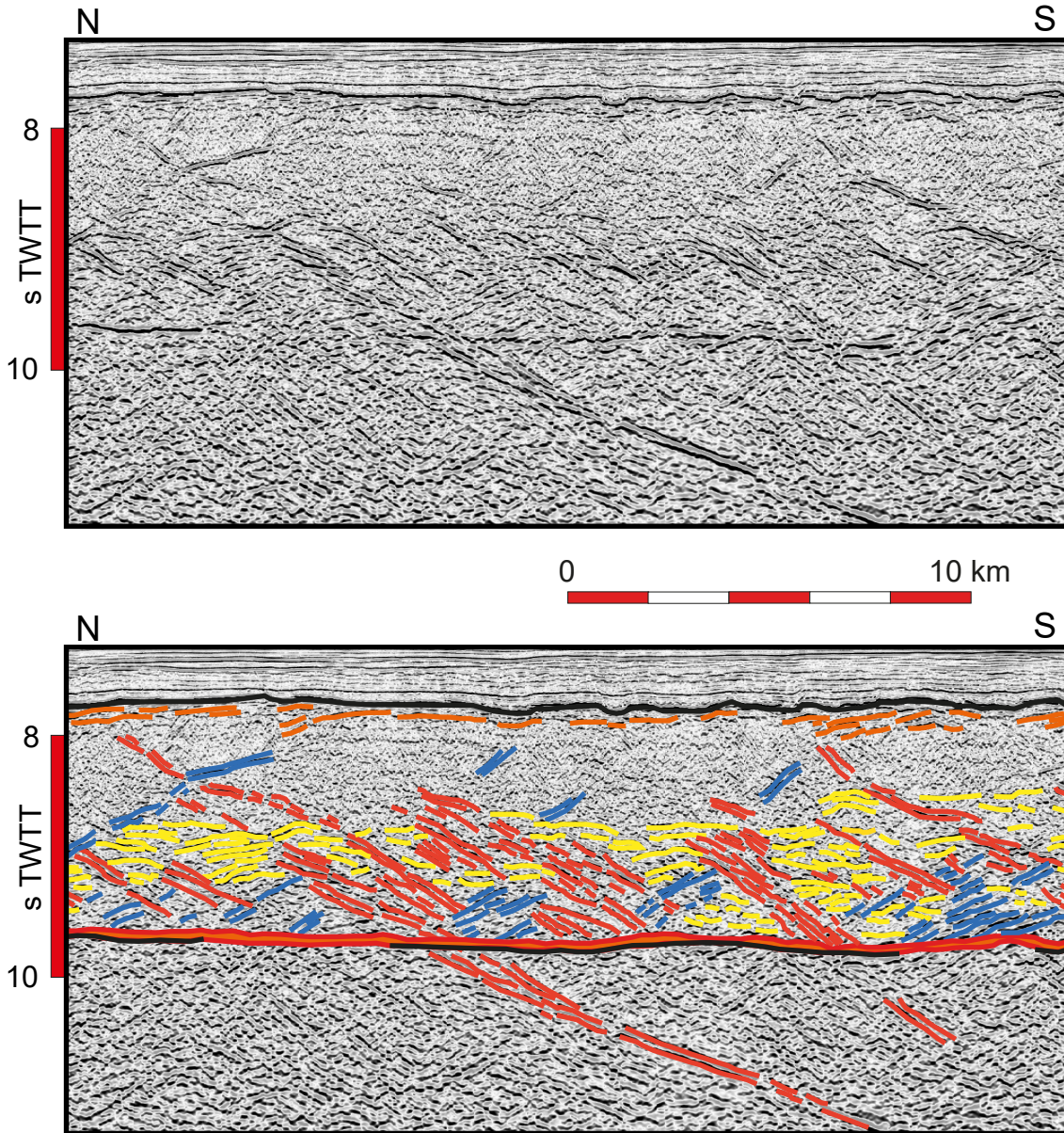


FIG. 6

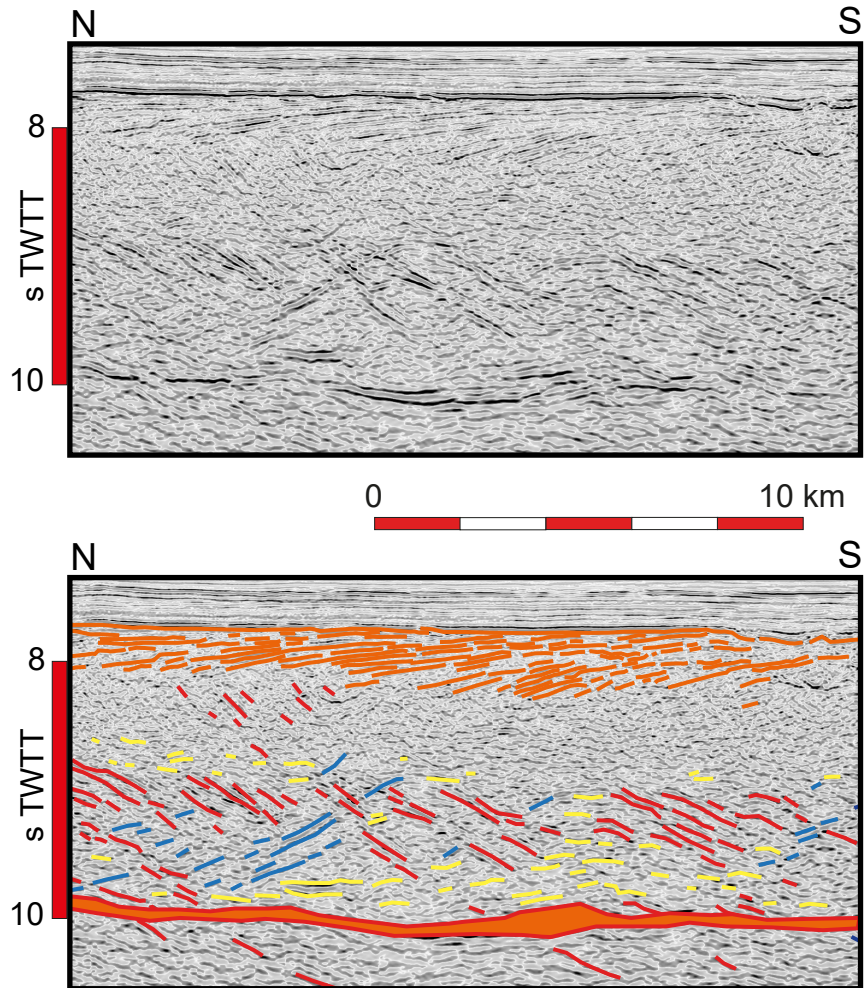




FIG. 7

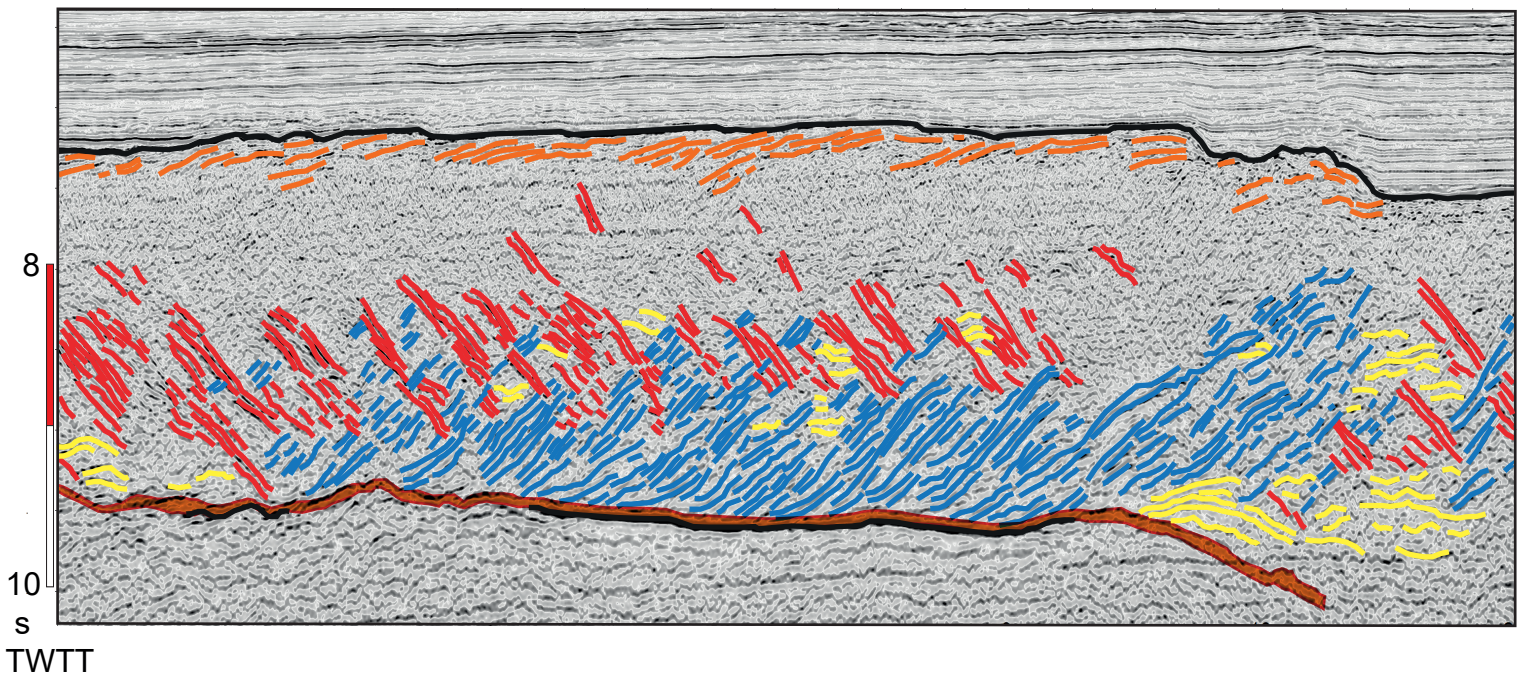
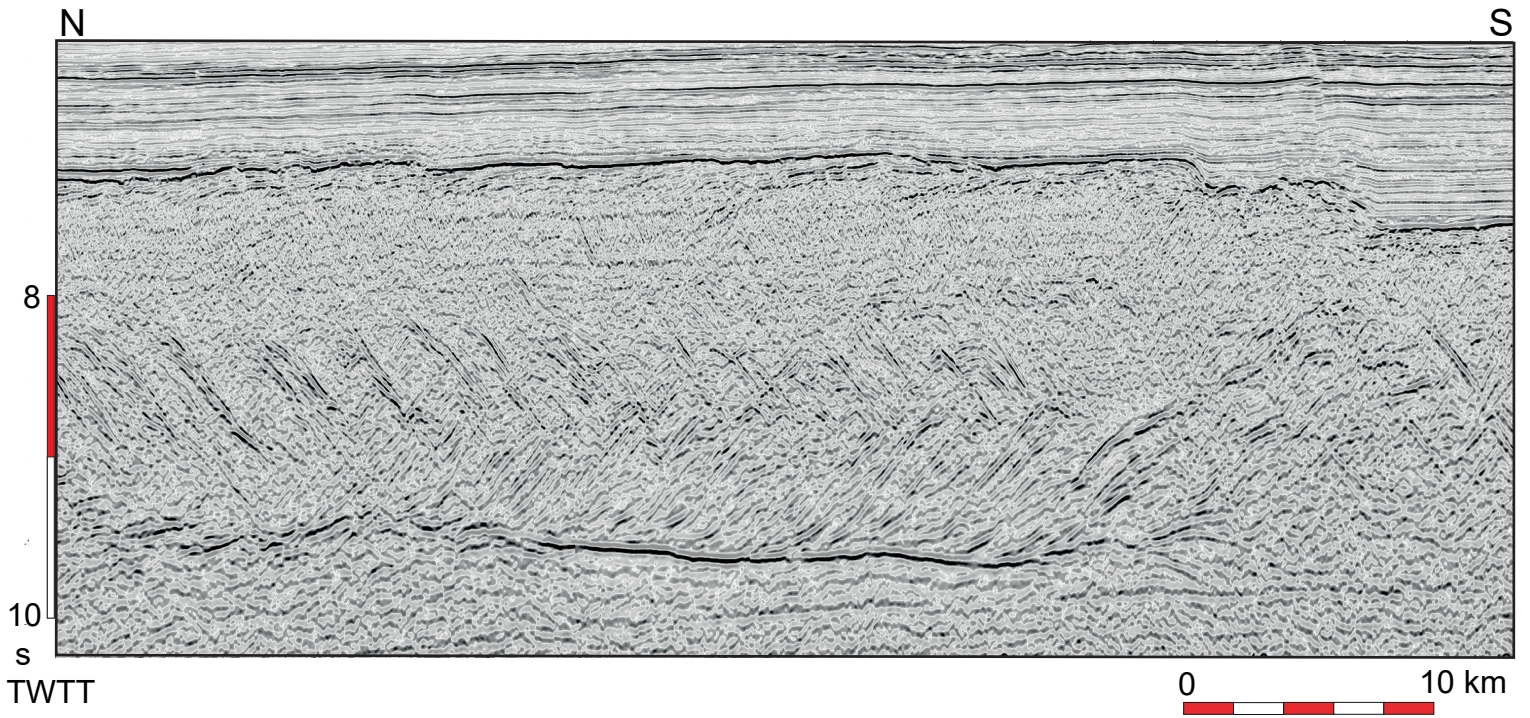




Fig. 8

